Improving Separation Control with Noise-Robust Variants of Dynamic Mode Decomposition

Maziar S. Hemati,[*]

Aerospace Engineering and Mechanics, University of Minnesota, Minneapolis, MN 55455, USA

Eric A. Deem [†]

Florida State University, Florida Center for Advanced Aero-Propulsion, Tallahassee, FL 32310, USA

Matthew O. Williams [‡]

Systems Department, United Technologies Research Center, East Hartford, CT 06118, USA

Clarence W. Rowley [§]

Mechanical and Aerospace Engineering, Princeton University, Princeton, NJ 08544, USA

Louis N. Cattafesta [¶]

Florida State University, Florida Center for Advanced Aero-Propulsion, Tallahassee, FL 32310, USA

Flow separation can lead to degraded performance in many engineered systems, which has led to sustained interest in developing strategies for suppressing and controlling flow separation. Separation control strategies based on open-loop forcing via synthetic jets have demonstrated a relative degree of success in various studies; however, many of these studies have relied upon trial-and-error "tuning" of a synthetic jet's operating parameters for satisfactory performance with respect to a particular flow configuration. Subsequent work has focused on improving the general understanding of fluid flow separation from a dynamical systems perspective, with the aim of isolating key mechanisms that can be exploited for more systematic controller designs. Numerical studies have shown that dynamically dominant flow characteristics, identified by the dynamic mode decomposition (DMD), can be used to guide the design of open-loop separation control strategies. While these approaches have proven valuable for dynamical analyses in numerics, standard formulations of DMD have recently been shown to possess systematic errors that can lead to misleading results when the data are corrupted by some degree of measurement noise (e.g., sensor noise in experimental studies). Here, we make use of DMD to synthesize time-resolved particle image velocimetry (TR-PIV) data from a canonical separation experiment in an effort to inform the design of open-loop separation control strategies; to this end, we make use of a noise-aware version of DMD—introduced in Hemati et al. (2015)—to assess the impact of measurement noise on the conclusions drawn for informing open-loop controller design. Additionally, we extend the noise-aware framework to formulate a noise-robust version of the streaming DMD algorithm presented in Hemati et al. (2014). Dynamic characterizations afforded by DMD-based techniques are then used to inform open-loop separation control strategies that are tested in experiments. We find that open-loop forcing at a frequency associated with the dominant DMD mode reduces the mean height of the separation bubble, suggesting that DMD-based techniques may provide a systematic means of designing open-loop control strategies aimed at suppressing flow separation.

[*]Assistant Professor, Aerospace Engineering and Mechanics, University of Minnesota, AIAA Member.
[†]Graduate Student, Mechanical Engineering, Florida State University, AIAA Student Member.
[‡]Senior Research Scientist, Systems Department, United Technologies Research Center.
[§]Professor, Mechanical and Aerospace Engineering, Princeton University, AIAA Associate Fellow.
[¶]Eminent Scholar & Professor, Mechanical Engineering, Florida State University, AIAA Associate Fellow.

American Institute of Aeronautics and Astronautics

Nomenclature

$\|\alpha\|$	DMD mode amplitude
λ	DMD eigenvalue
φ	DMD mode
c	Plate chord-length
h	Plate thickness
m	Number of snapshots
n	Snapshot dimension
A	DMD operator
Re_c	Reynolds number with respect to chord
X, Y	Snapshot data matrices
Z	Augmented snapshot data matrix

I.   Introduction

Flow separation can lead to degraded performance in many engineered systems (e.g., decreased lift, increased drag, reduced efficiency). As such, there has been growing interest in strategies aimed at suppressing and controlling flow separation. Numerous active flow control strategies have been proposed to modify the fluid dynamics in a favorable way. Owing to their relative simplicity, open-loop control strategies have been among the more popular approaches adopted for active separation control. Many recent open-loop strategies have aimed at forcing the flow at an "optimal" frequency—often determined by trial-and-error—using a variety of zero-net-mass-flux (ZNMF) actuation devices, including synthetic jets [1, 2, 3, 4, 5] and plasma actuators [6, 7, 8, 9, 10].

While ZNMF actuation strategies have been demonstrated to effectively alter the flow in a desirable manner, the trial-and-error tuning of these controllers often fails to offer insights about why the control strategy chosen is effective, which can impede the design of more effective controllers in the future. Of course, more systematic and targeted approaches to separation control will require a better understanding of the nonlinear fluid dynamics involved in flow separation. In response to this need, recent efforts have sought to gain a better understanding of the underlying flow mechanisms involved in flow separation through systematic studies of a canonical flow separation configuration [11, 12, 13]. The canonical separation configuration (Figure 1) was developed to provide a convenient environment to study flow separation—both numerically and experimentally—without concern for ancillary effects, such as body curvature. The configuration allows the size and location of the separation bubble to be prescribed, thus enabling systematic study of flow separation. Numerical [12, 13, 14] and experimental [15] studies of the canonical configuration have led to the identification of three characteristic frequencies relevant to flow separation: (1) the shear layer frequency, (2) the separation bubble frequency, and (3) the wake frequency. Additionally, these studies provided evidence for lock-on between frequencies in certain flow regimes, highlighting the possibilities for nonlinear flow interactions that could be exploited for separation control.

In extracting the characteristic frequencies associated with the canonical flow separation problem, these studies relied upon spectral analyses of individual probe signals from the wake, shear layer, and separation bubble; however, as noted in Tu et al. (2014), the spectra computed from probe data are sensitive to probe locations. For instance, in numerical simulations, the spectrum computed from a probe at one point in the shear layer gives a different frequency peak than the same probe moved slightly upstream [14]. To overcome the issue of sensitivity due to probe location, Tu et al. proposed using Koopman spectral analysis and the dynamic mode decomposition (DMD) to extract spectra from *snapshots* of the flow, thus providing a "more global" description of the dynamics [14]. DMD analysis of numerical simulation data identified characteristic flow frequencies, along with their associated dynamic spatial modes; the DMD modes—spatial structures with simple linear dynamics characterized by the associated DMD eigenvalues—allowed frequency peaks to be related to the wake, shear layer, separation bubble, or some combination thereof. The dynamics characterized by the DMD analysis were then used to guide the design of an improved open-loop ZNMF controller, as reported in [14].

Despite DMD's success in informing and guiding open-loop controller design based on snapshot data

taken from numerical simulations, standard DMD techniques will not necessarily achieve a similar degree of success if the snapshot data are subject to measurement uncertainties, as is the case in experiments. In fact, as was recently shown in [16, 17], when applied to noisy data, standard formulations of DMD may result in noise-induced biases—due to an asymmetric treatment of measurement noise—that can lead to erroneous characterizations of the relevant dynamics. In the context of separation control, this implies that open-loop controllers that have been designed based on the insights offered by conventional DMD analysis of experimentally measured snapshot data may be misinformed and misdirected.

In the present study, we are interested in using DMD to study flow separation in experiments, so considerations of measurement noise corruption will be important. Snapshot data—captured via time-resolved particle image velocimetry (TR-PIV)—will be analyzed using a de-biased/noise-aware formulation of DMD [16, 17], which will enable the identification of dominant separated flow dynamics that can be targeted by an open-loop controller. While our studies indicate that the standard formulation of DMD is able to identify the dominant dynamics relevant to informing effective open-loop forcing strategies, the noise-aware analysis suggests that standard DMD poorly characterizes some of the less dominant flow dynamics. Here, we also study the utility of the streaming DMD algorithm [18] for guiding the design of open-loop separation control strategies. We find that the streaming DMD method fails to provide interpretable insights with regards to our TR-PIV datasets, making it an inadequate analysis technique for reliably informing controller design. In an effort to reconcile this deficiency, we extend the noise-aware formulation of DMD to the streaming context, yielding a noise-robust streaming DMD algorithm that successfully captures the relevant flow dynamics in a low-storage manner suitable for analyzing large and streaming datasets that are subject to measurement noise. We note that software implementations of various DMD analysis techniques [16, 18, 19, 20], including the noise-aware streaming DMD technique introduced here, are freely available from [21]. As we will show, the de-biased/noise-aware variants of DMD prove valuable in targeting relevant flow dynamics via open-loop ZNMF forcing.

II.   Experimental Setup

All experiments conducted for this study were held in the Florida State Flow Control (FSFC) wind tunnel. The FSFC is an open-return wind tunnel with test section area of 30.5 cm × 30.5 cm and a length of 61.0 cm.

The chord of the plate is $c = 402$ mm, the span is $s = 305$ mm, and the height is $h = 0.095c$. The leading edge profile of the plate is a 4:1 ellipse and the trailing edge is square. The freestream velocity is $U_\infty = 3.9$ m/s and is monitored by a pitot static probe mounted upstream of the test section. The Reynolds number for these experiments is $Re_c = 10^5$, therefore the boundary layer is likely laminar upstream of the separation point.

To generate the canonical separated flow over the flat plate model, an adverse pressure gradient is generated by a suction/blowing boundary condition imposed on the ceiling of the wind tunnel test section. The boundary condition is maintained by a closed return duct system in which the flow rate is controlled by a variable speed fan. The maximum suction velocity through the entrance of the duct is $0.32U_\infty$, and the maximum blowing velocity at the outlet is $0.31U_\infty$. The location of the plate relative to the ceiling is such that the average separation bubble length is $x_{sep} = 0.20c$.

More information regarding the separation system, flat plate model, and ZNMF actuators can be found in [15]. A schematic of the plate with relevant dimensions is shown in Figure 1.

II.A.   Open-Loop Actuation

A rectangular slot Zero-Net-Mass-Flux (ZNMF) jet actuator is embedded within the upper surface of the plate. This device operates by the successive ingestion and expulsion of the surrounding fluid such that a non-zero time-averaged momentum flux is generated—with zero time-averaged mass flux [22]. Actuation is achieved by varying the volume of a cavity beneath the slot using four piezoelectric disks, (APC Inc., PZT5J, Part Number: P412013T-JB). The disks are oriented spanwise along the lower surface of the cavity.

A burst modulated waveform with a 50% duty cycle drives the actuator. The actuator waveform consists of a burst frequency and a carrier frequency. The carrier frequency is chosen to be near a resonant peak of the actuator and is much higher than the characteristic frequencies of the flow. This carrier frequency is cycled on and off impulsively at the burst frequency f_b. An illustration of the burst modulation waveform
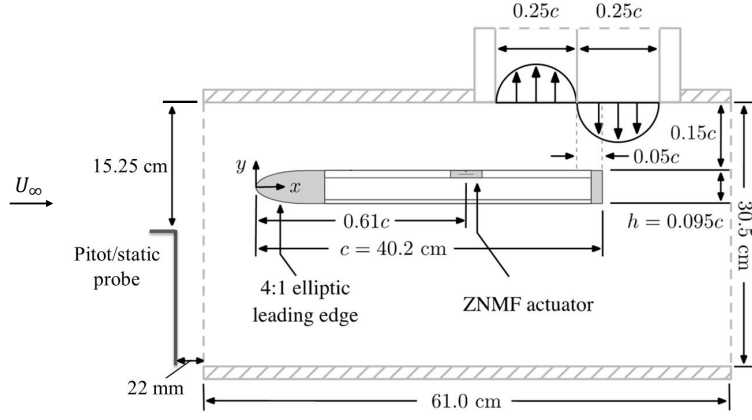
American Institute of Aeronautics and Astronautics

Figure 1: Schematic of the flat plate model and flow separation system.
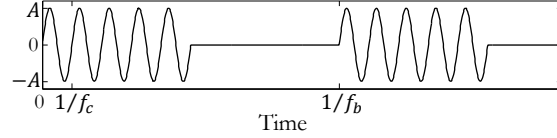
is provided in Figure 2.

Figure 2: Burst modulation waveform used for actuation.

For these experiments, the carrier frequency is fixed at $f_c = 2050$ Hz. The driving amplitude is also held constant at $A = 30$ V. This provides a nominal momentum coefficient of $c_\mu = 0.51 \times 10^{-3}$, in which

$$c_\mu = \frac{A_j v_{rms}^2}{A_{sep} U_\infty^2}. \tag{1}$$

In this definition, A_j is the area of the actuator slot, and A_{sep} is the separation region planform area (the length of the separation region, x_{sep} multiplied by the span of the flat plate). The rms velocity of the actuator is determined by hotwire anemometry, in which the hotwire probe is placed at the exit plane of the actuator slot.

II.B.   Time-Resolved PIV

Time-Resolved Particle Image Velocimetry (TR-PIV) measurements of the separated flow are acquired. The measurement plane is oriented streamwise and vertical, grazing the top surface of the flat plate (see Figure 3). The flow is seeded with olive oil particles by a TSI 9307-6 oil droplet generator. The nominal size of the olive oil particles is 1 μm [23]. Images of the illuminated particles are acquired by a Phantom v411 high speed camera. The particles are illuminated by a New Wave Pegasus SN 60022 Nd-YLF laser operating in a double-pulse, frame-straddle configuration. This results in one PIV vector field per every two image acquisitions. The images are acquired at 3200 fps, therefore the TR-PIV vector acquisition rate is 1600 Hz. The time between the laser pulses for a single TR-PIV acquisition is $\Delta t = 180 \mu s$.
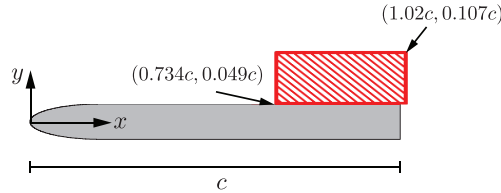

Figure 3: The measurement plane, depicted by the red box in this schematic, is oriented streamwise and vertical, grazing the top surface of the flat plate.

American Institute of Aeronautics and Astronautics

Once images are acquired, image preprocessing and vector calculations are performed within LaVision DaVis ver 8.1.x [24]. For image preprocessing, a sliding background subtraction filter is employed in order to reduce background image contamination. Then, a particle intensity normalization is applied to reduce non-uniform illumination. A direct cross-correlation is performed among interrogation windows of the image pairs to determine the particle shift. This process is iterated for successively smaller interrogation windows. The final interrogation window size is 16×16 pixels with 75 % overlap, which results in a vector resolution of 0.466 mm per vector.

III.   Dynamic Mode Decomposition of Separated Flow TR-PIV Data

The dynamic mode decomposition (DMD)—a data-driven dynamical systems analysis technique that was first introduced in the fluid mechanics community [25, 26]—can be used to help characterize the dominant dynamics of a separated flow, thus informing the design of an open-loop control strategy. DMD processes snapshot data, measured from a system at various instants in time, to yield a spatiotemporal decomposition in terms of a set of spatial modes and their associated temporal (dynamical) characteristics. The decomposition amounts to the eigendecomposition of a linear operator that maps snapshots $x(t_k) \in \mathbb{R}^n$ to their time-shifted counterparts $x(t_k + \Delta t) \in \mathbb{R}^n$. In practice, m snapshot pairs are sorted column-wise into the snapshot data matrices X and Y,

$$ X \quad := \quad \begin{bmatrix} x(t_1) & x(t_2) & \cdots & x(t_m) \end{bmatrix} \in \mathbb{R}^{n \times m} \tag{2} $$

$$ Y \quad := \quad \begin{bmatrix} x(t_1 + \Delta t) & x(t_2 + \Delta t) & \cdots & x(t_m + \Delta t) \end{bmatrix} \in \mathbb{R}^{n \times m} \tag{3} $$

Then, based on the definition in [27], the DMD modes and eigenvalues correspond to the eigendecomposition of the best-fit/minimum-norm linear operator

$$ A := YX^+ \in \mathbb{R}^{n \times n}. \tag{4} $$

Rather than computing the eigendecomposition of $A \in \mathbb{R}^{n \times n}$, which can be computationally impractical, the *standard DMD* algorithm works with a lower-dimensional proxy system $\tilde{A} \in \mathbb{R}^{r \times r}$, as described below [27].

Standard DMD:

1. Compute the (reduced) SVD of $X = U_r \Sigma_r V_r^*$, where $r = \mathrm{rank}(X)$.

2. Construct the lower-dimensional proxy system $\tilde{A} := U_r^* Y V_r \Sigma_r^{-1} \in \mathbb{R}^{r \times r}$.

3. Compute the eigendecomposition of the proxy system, $\tilde{A} w_i = \lambda_i w_i$.

4. The non-zero DMD eigenvalues are given by λ_i, while the corresponding DMD modes are computed as $\varphi_i = U_r w_i$.

The decomposition into dynamic modes φ_i and eigenvalues λ_i provides a spatiotemporal description of the flow that can be used to inform open-loop controller design; insights about the dynamical characteristics of the flow, afforded by DMD analysis, can be used for targeted control strategies. Further discussion of open-loop controller design follows in Section V.

While DMD's potential to offer insights about a fluid flow is quite appealing, practitioners have noted sensitivity of the decomposition to measurement noise when DMD is applied to data gathered from physical experiments. In an effort to deal with this sensitivity, numerous forms of ensemble averaging, cross-validation, rank-reduction, and windowing have been employed [18, 26, 27, 28, 29, 30, 31, 32, 33]; however, as shown in [16], such strategies actually yield a biased analysis—owing to an asymmetric treatment of "inexact" data by standard DMD. In fact, this bias is quantifiable and, given knowledge of the noise characteristics, can be corrected for [17]. Without prior knowledge of the noise characteristics, the total least-squares perspective of DMD can be invoked to de-bias the ensuing analysis instead [16]. Doing so amounts to a pre-processing stage that consists of projecting the data onto a subspace determined from an augmented snapshot matrix

$$ Z := \begin{bmatrix} X \\ Y \end{bmatrix}, \tag{5} $$

such that the snapshot data in both X and Y are taken into consideration when determining the lower-dimensional subspace for projection. Upon projecting the snapshot data onto an appropriate basis, the standard DMD algorithm can then be applied to the resulting "corrected" snapshot data to yield a de-baised characterization of the dynamics. While it is intuitive to think about these stages separately, an algorithmically equivalent *total DMD (TDMD)* procedure consists of the steps outlined below.

Total DMD:

1. Compute (reduced/truncated) SVD of $Z = U_r \Sigma_r V_r^*$.

2. Compute the SVD of the "corrected" data $\bar{X} = X V_r V_r^* = \bar{U} \bar{\Sigma} \bar{V}^*$.

3. Construct the de-biased proxy system $\bar{A} := \bar{U}^* Y \bar{V} \bar{\Sigma}^{-1} \in \mathbb{R}^{r \times r}$.

4. Perform the eigendecomposition $\bar{A} w_i = \lambda_i w_i$.

5. The non-zero DMD eigenvalues are given by λ_i, while the corresponding DMD modes are computed as $\varphi_i = \bar{U} w_i$.

We defer details of the formulation and properties of noise-aware techniques to [16] and [17]. We note that the de-biasing framework is generalizable to other DMD-based techniques as well (e.g., streaming DMD [18], optimal mode decomposition [33], and sparsity-promoting DMD [34]). In the next section, we will consider extensions to the streaming technique in more detail.

Here, we apply both standard DMD and TDMD to the TR-PIV snapshots of the velocity field in order to assess the differences between the two techniques in determining a candidate set of forcing frequencies for open-loop separation control. DMD modes resulting from these analyses can reveal dynamical interplays between the shear layer, separation bubble, and wake (see Figure 4), which will ultimately inform the design of the open-loop forcing strategy.
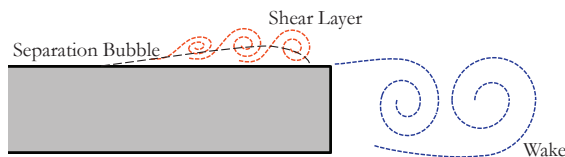

Figure 4: The shear layer, separation bubble, and wake are active regions of the flow with coupled dynamics. A better understanding of the dynamical interplays between these flow modes can help develop targeted strategies for separation control.

The TR-PIV dataset for the uncontrolled, canonical separated flow ($Re_c = 10^5$) studied here consists of $m = 3000$ snapshot pairs, each with snapshot dimension $n = 42\,978$. The spectra and mode amplitudes computed from standard DMD and TDMD are presented in Figure 5. While the dynamics identified by TDMD are less damped than those identified by standard DMD, the dominant frequencies are more or less consistent between the two methods. Significant differences only seem to arise in the range 45 Hz–75 Hz, indicating that measurement noise may only influence the characterization of less dominant dynamics in the experimental data considered here. Further, while both methods seem to give similar mode shapes over most of the spectrum (see the vorticity modes extracted by each method in Figure 6), some noteable differences do arise: for example, in comparing mode shapes, TDMD indicates that the upstream portion of the shear layer may play a prominent role at 17 Hz, whereas standard DMD provides no such indication. In Section V, the influence of each of the candidate DMD/TDMD frequencies will be studied in the context of open-loop forcing. For the configuration studied here, the 106 Hz mode—successfully captured by both standard DMD and TDMD—turns out to be most influential on decreasing the height of the separation bubble. As such, if one is only interested in determining a candidate set of frequencies for reducing the height of the separation bubble during open-loop forcing, it appears that there is little gain in performing TDMD over standard DMD; however, further investigation will be needed to determine whether this is true in other flow regimes

American Institute of Aeronautics and Astronautics

as well.

(a) Spectra
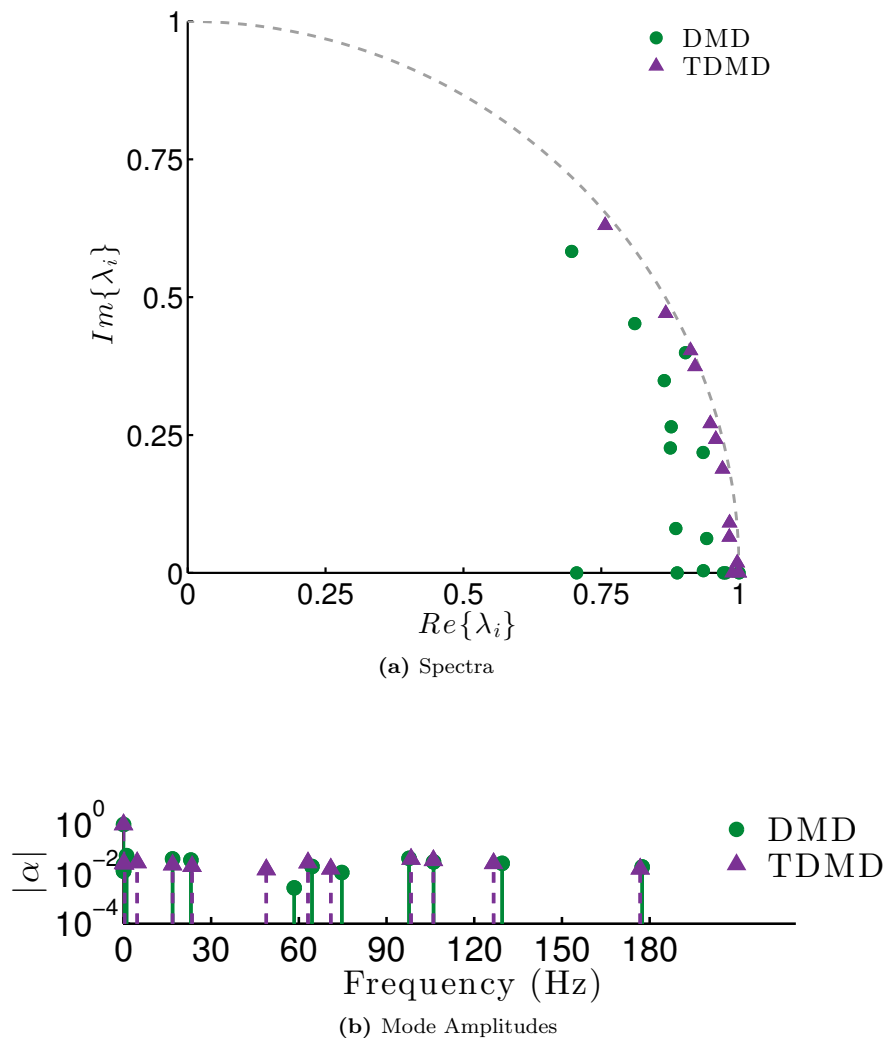

(b) Mode Amplitudes

Figure 5: TDMD predicts smaller decay rates than DMD for the oscillatory modes that are extracted from TR-PIV data in a separated flow experiment. DMD and TDMD eigenvalues are plotted in (a) as circles and triangles, respectively. Mode amplitudes are normalized by the maximum amplitude and plotted versus frequency in (b).

IV. Dynamic Mode Decomposition of Large and Streaming Datasets

In the previous section, DMD and TDMD were both able to process TR-PIV data from our canonical separation experiment—with number of snapshot pairs $m = 3000$ and snapshot dimension $n = 42\,978$—to extract a candidate set of forcing frequencies for open-loop control. As is the case here, when noise is a relevant consideration, it is often advisable to increase the number of snapshots in order to reduce the influence of noise as much as possible: noise-aware algorithms, such as TDMD, are expected to yield improved dynamical representations with the inclusion of more and more snapshots (i.e., as $m \to \infty$) [16, 17]. Of course, the TDMD algorithm invoked previously was formulated for use as a batch-processing technique—i.e., all of the snapshots must be processed in a single invocation of the algorithm—which can be impractical for performing a dynamical analysis of large datasets that are composed of many snapshots. With this limitation in mind, in the present section, we formulate a "streaming" variant of TDMD that provides a computation-

American Institute of Aeronautics and Astronautics

DMD   **TDMD**

(a) $f = 177$ Hz, $|\lambda| = 0.91$, $|\alpha| = 0.02$ **(j)** $f = 177$ Hz, $|\lambda| = 0.99$, $|\alpha| = 0.02$

(b) $f = 130$ Hz, $|\lambda| = 0.93$, $|\alpha| = 0.03$ **(k)** $f = 127$ Hz, $|\lambda| = 0.99$, $|\alpha| = 0.03$

(c) $f = 106$ Hz, $|\lambda| = 0.99$, $|\alpha| = 0.03$ **(l)** $f = 106$ Hz, $|\lambda| = 1.0$, $|\alpha| = 0.04$

(d) $f = 98$ Hz, $|\lambda| = 0.93$, $|\alpha| = 0.04$ **(m)** $f = 98$ Hz, $|\lambda| = 0.99$, $|\alpha| = 0.04$

(e) $f = 75$ Hz, $|\lambda| = 0.92$, $|\alpha| = 0.01$ **(n)** $f = 71$ Hz, $|\lambda| = 0.99$, $|\alpha| = 0.02$

(f) $f = 65$ Hz, $|\lambda| = 0.90$, $|\alpha| = 0.02$ **(o)** $f = 63$ Hz, $|\lambda| = 0.99$, $|\alpha| = 0.03$

(g) $f = 58$ Hz, $|\lambda| = 0.96$, $|\alpha| = 0.003$ **(p)** $f = 49$ Hz, $|\lambda| = 0.99$, $|\alpha| = 0.02$

(h) $f = 23$ Hz, $|\lambda| = 0.89$, $|\alpha| = 0.04$ **(q)** $f = 23$ Hz, $|\lambda| = 0.99$, $|\alpha| = 0.02$

(i) $f = 17$ Hz, $|\lambda| = 0.94$, $|\alpha| = 0.04$ **(r)** $f = 17$ Hz, $|\lambda| = 0.98$, $|\alpha| = 0.02$
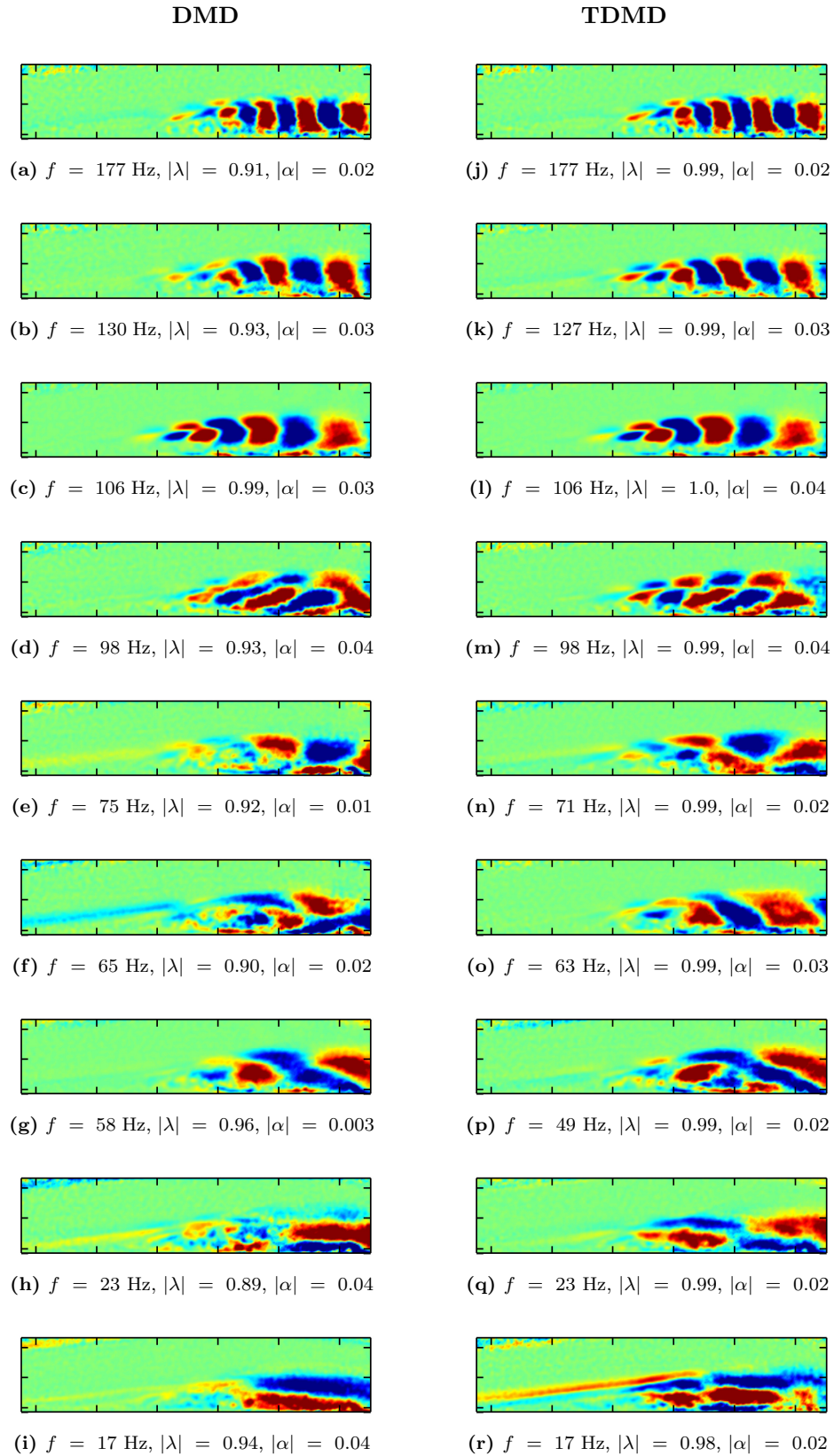
Figure 6: A comparison of TDMD modes with DMD modes suggests that some aspects of the separated flow dynamics may be characterized by different spatial structures than revealed by standard DMD; while many TDMD modes are qualitatively similar to DMD modes, some of the modes differ. The oscillatory vorticity modes are plotted top to bottom in order of decreasing frequency for DMD (a)–(i) and TDMD (j)–(r). Here, $r = 25$ and modes of vorticity are computed from DMD/TDMD modes of velocity.

American Institute of Aeronautics and Astronautics

ally tractable means of analyzing large datasets consisting of many snapshots. The streaming formulation of TDMD introduced here is a low-storage single-pass algorithm—akin to the streaming DMD (SDMD) method introduced in [18]—designed to yield relevant dynamical analyses of datasets composed of arbitrarily many snapshot pairs; in fact, the streaming TDMD (STDMD) algorithm formulated here can also be used to analyze datastreams (i.e., $m \to \infty$) "on the fly", which may be useful in developing closed-loop separation control architectures in future work (c.f., [35]). As we will show, dominant dynamics extracted by STDMD reasonably approximate those identified by TDMD in batch-processing mode. Moreover, STDMD outperforms the original SDMD technique in extracting relevant dynamical information from TR-PIV data from the separated flow experiments in this study, since robustness to noise has been suitably considered in the formulation.

To derive STDMD, we begin by taking the QR-decomposition of the augmented snapshot matrix

$$Z := \left[\begin{array}{c} X \\ Y \end{array} \right] = Q_z R_z, \tag{6}$$

such that

$$X = \left[\begin{array}{cc} I & 0 \end{array} \right] Q_z R_z \tag{7}$$

$$Y = \left[\begin{array}{cc} 0 & I \end{array} \right] Q_z R_z. \tag{8}$$

We will also require an additional QR-factorization based on this,

$$\left[\begin{array}{cc} I & 0 \end{array} \right] Q_z R_z = Q_x R_x. \tag{9}$$

Upon substitution of expressions into the definition of the DMD operator $A := Y X^+$, as defined in [27], and invoking the identity $P^+ = P^* \left(P P^* \right)^+$,

$$A = \left[\begin{array}{cc} 0 & I \end{array} \right] Q_z G_z Q_z^* \left[\begin{array}{c} I \\ 0 \end{array} \right] Q_x G_x^+ Q_x^*, \tag{10}$$

where $G_z := R_z R_z^*$ and $G_x := R_x G_z R_x^*$. While (10) provides a useful expression for the DMD operator that can be updated incrementally as new snapshots are made available, it is more computationally tractable to work on the low-dimensional version $\tilde{A}$ via Q_x—the de-biased orthonormal basis for the image of X—as

$$\tilde{A} := Q_x^* \left[\begin{array}{cc} 0 & I \end{array} \right] Q_z G_z Q_z^* \left[\begin{array}{c} I \\ 0 \end{array} \right] Q_x G_x^+. \tag{11}$$

As in SDMD, while this expression looks more complicated than its batch-processed counterpart, the number of snapshots m no longer appears as a dimension of any of the terms, so the algorithm remains low-storage regardless how many snapshots are considered. Additionally, this final expression is analogous to the SDMD expression introduced in [18], and so the updating procedure follows similarly. Software implementations of this method are freely available for download from [21].

Here, we apply both streaming algorithms to the same TR-PIV dataset that was analyzed with the batch-processing techniques in Section III; the resulting spectra are presented in Figure 7. STDMD identifies a spectrum that more closely resembles the spectra computed by each of the batch processed methods, whereas SDMD seems inconsistent with these other analysis procedures. The damped nature of eigenvalues aside, STDMD also seems to more closely capture the frequency spectrum of the batch-processed algorithms when compared to SDMD. Of course, neither of the streaming methods is expected to reproduce the results from the batch-processed computations exactly: by construction of a low-storage procedure, both streaming techniques make repeated use of a data-compression stage to maintain low-rank. While the resulting streaming analyses are not necessarily equivalent to their batch-processing counterparts, it was shown in [18] that streaming DMD and similar algorithms can still provide useful and interpretable insights with regards to the dominant dynamics. For example, often only the general shape of a DMD mode is needed to gain insights about the spatial structures that play a role in the dynamic evolution of a flow. In the present case, the interpretability of STDMD modes far exceeds the interpretability of the SDMD modes (see Figure 8). STDMD captures

American Institute of Aeronautics and Astronautics

similar spatial structures as both batch-processing techniques, while SDMD fails to do so. While SDMD seems to capture some coherence in its 104Hz mode (see tile (d) in Figure 8), this information would have been insufficient to reliably inform open-loop control design had the alternative analyses not been performed in conjunction with this one.
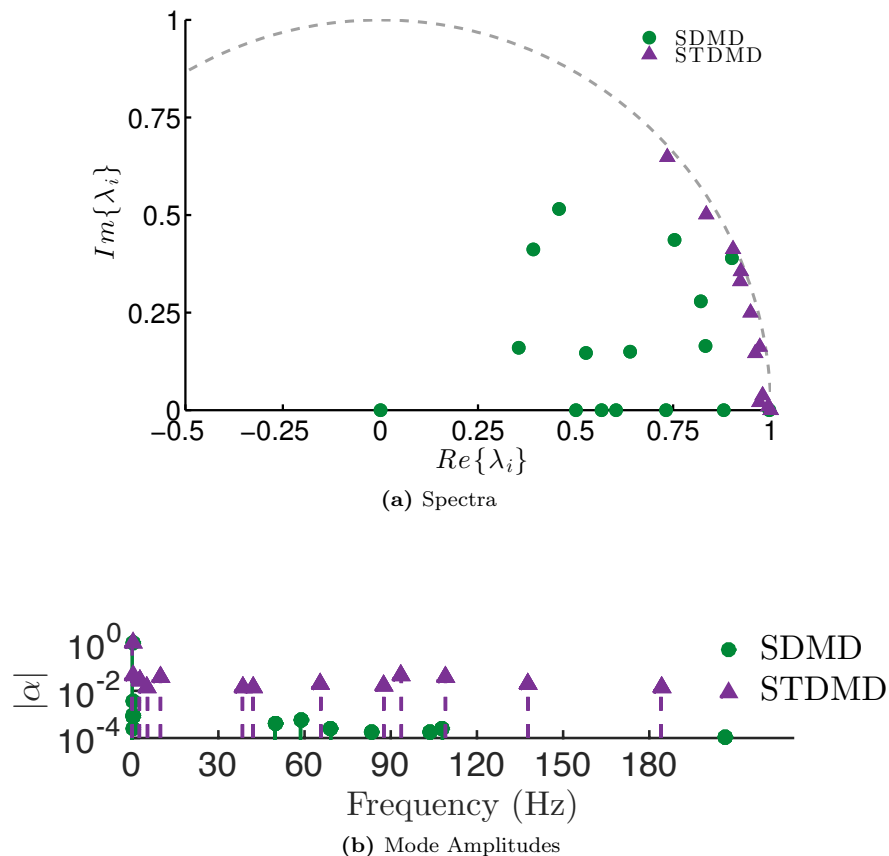

(a) Spectra

(b) Mode Amplitudes

Figure 7: STDMD predicts smaller decay rates than SDMD for the oscillatory modes that are extracted from TR-PIV data in a separated flow experiment. SDMD and STDMD eigenvalues are plotted in (a) as circles and triangles, respectively. Mode amplitudes are normalized by the maximum amplitude and plotted versus frequency in (b).

V.   Dynamic Mode Decomposition for Open-Loop Control Design

Targeting the natural dynamics of separated flow has been shown to be an effective strategy for reducing separation. In [15], the power spectral density of point pressure measurements were used to identify interesting dynamics of the separated flow, which were then used to inform open-loop control strategies. It was found that open-loop control performance was greatly improved when the actuation frequency was approximately equal to the measured shear layer frequency. In the present work, we opt to make use of the full flowfield to inform open-loop controller design by drawing upon insights afforded by variants of DMD, as presented
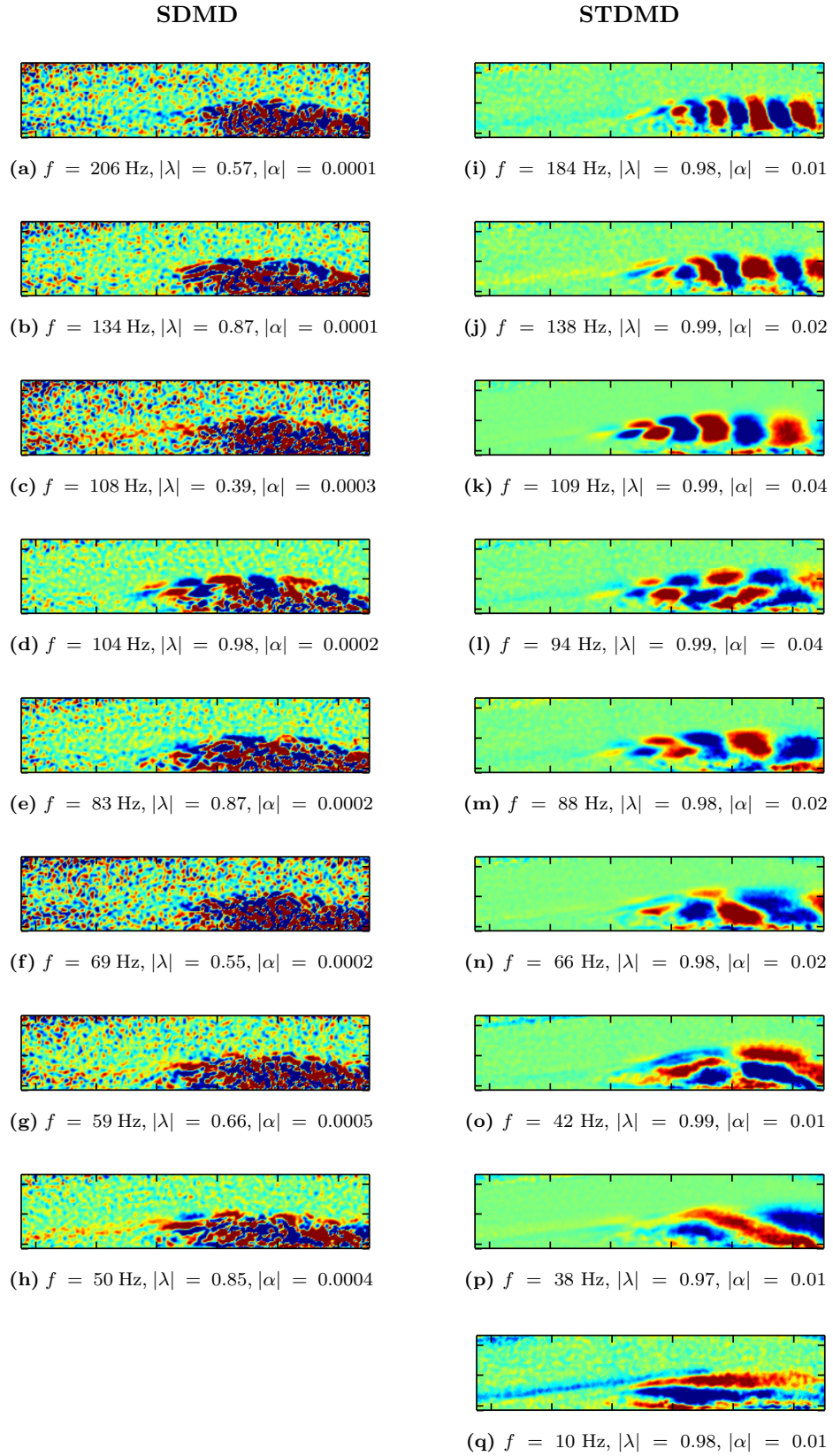
(a) $f = 206\,\text{Hz}, |\lambda| = 0.57, |\alpha| = 0.0001$

(i) $f = 184\,\text{Hz}, |\lambda| = 0.98, |\alpha| = 0.01$

(b) $f = 134\,\text{Hz}, |\lambda| = 0.87, |\alpha| = 0.0001$

(j) $f = 138\,\text{Hz}, |\lambda| = 0.99, |\alpha| = 0.02$

(c) $f = 108\,\text{Hz}, |\lambda| = 0.39, |\alpha| = 0.0003$

(k) $f = 109\,\text{Hz}, |\lambda| = 0.99, |\alpha| = 0.04$

(d) $f = 104\,\text{Hz}, |\lambda| = 0.98, |\alpha| = 0.0002$

(l) $f = 94\,\text{Hz}, |\lambda| = 0.99, |\alpha| = 0.04$

(e) $f = 83\,\text{Hz}, |\lambda| = 0.87, |\alpha| = 0.0002$

(m) $f = 88\,\text{Hz}, |\lambda| = 0.98, |\alpha| = 0.02$

(f) $f = 69\,\text{Hz}, |\lambda| = 0.55, |\alpha| = 0.0002$

(n) $f = 66\,\text{Hz}, |\lambda| = 0.98, |\alpha| = 0.02$

(g) $f = 59\,\text{Hz}, |\lambda| = 0.66, |\alpha| = 0.0005$

(o) $f = 42\,\text{Hz}, |\lambda| = 0.99, |\alpha| = 0.01$

(h) $f = 50\,\text{Hz}, |\lambda| = 0.85, |\alpha| = 0.0004$

(p) $f = 38\,\text{Hz}, |\lambda| = 0.97, |\alpha| = 0.01$

(q) $f = 10\,\text{Hz}, |\lambda| = 0.98, |\alpha| = 0.01$

Figure 8: A comparison of STDMD modes with SDMD modes shows that the noise-aware framework significantly improves the extraction of relevant dynamics from TR-PIV data in a separated flow experiment. The dominant oscillatory modes are plotted top to bottom in order of decreasing frequency for SDMD (a)–(h) and STDMD (i)–(q). Here, $r = 25$ and modes of vorticity are computed from SDMD/STDMD modes of velocity.

American Institute of Aeronautics and Astronautics

in previous sections. Whereas the frequencies measured from individual probes can be highly sensitive to probe location, a snapshot-based analysis procedure can offer insights by synthesizing measurements from many locations in the flowfield simultaneously.

In previous sections, we reported the dominant dynamics extracted from snapshots of the velocity-field using variants of DMD, including noise-aware and streaming formulations. Here, we report results from open-loop actuation experiments that target the natural frequencies identified by DMD and its variants; that is, the DMD analyses are used to establish a set of candidate frequencies for ensuing open-loop actuation studies. By studying the mode shapes in conjunction with the dominant dynamics, specific dynamical regimes of the flow can be targeted (e.g., shear layer, separation bubble, wake), which in turn allows for the development of tailored control strategies based on the receptivity of these modes to fluidic actuation.

If we consider the forcing frequencies identified by TDMD, in which the proxy system has dimension $r = 25$, then we arrive at a set of nine distinct candidate forcing frequencies to study. This is narrowed down further by beginning with high-amplitude modes. These frequencies correspond to the right column of Figure 6. In the remainder, we present results associated with open-loop forcing at each of these candidate frequencies, demonstrating that forcing at the dominant DMD frequency reduces the size of the separation bubble most effectively. We note that in this study, although the driving amplitude is fixed, the momentum coefficient does vary within this range of forcing frequencies. The absolute value of this variance is 0.21×10^{-3}. For future studies, the driving amplitude will be adjusted to keep the momentum coefficient constant.

As a performance metric, the height of the mean reversed flow region is computed for each forcing frequency (i.e., an indication for the size of the separation bubble) and plotted in Figure 9. With the aim of
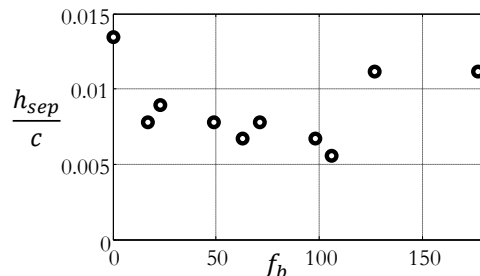

Figure 9: Normalized mean separation height plotted against input frequency. $f_b = 0$ corresponds to the uncontrolled baseline separation height. The minimum mean separation height measured corresponds to forcing at the dominant frequency identified by TDMD, 106 Hz.

reducing the separation region, the 106 Hz forcing frequency exhibits the greatest performance. Also, from Figure 6, the 106 Hz mode has the highest amplitude of all candidate modes. This mode likely corresponds to the shear layer frequency [15], though more rigorous analysis is warranted to corroborate this claim.

Interestingly, the separation height rapidly increases for $f_b = 127$ Hz. A plot containing the mean vorticity fields, superimposed with the line corresponding to $\bar{u}/U_\infty = 0$ for the baseline separation and 106 Hz and 127 Hz forcing frequency cases is provided in Figure 10.

It seems that choosing the actuation based on the frequency of the DMD mode with the highest oscillation amplitude results in the most reduction of the mean separation region. In a linear systems sense, this would be analogous to forcing at the most amplified resonant frequency. The nonlinear extension of this is that this DMD mode describes the most dominant component of the natural limit cycle of the baseline separated flow. Thus, forcing this component results in the most drastic deviation from the baseline dynamics. In this case, this manifests as a reduction in the mean separation region.

Select instantaneous vorticity snapshots are provided in Figure 11. These plots provide some insight regarding the shear layer dynamics subject to 106 Hz and 127 Hz forcing. The baseline separation exhibits coherent vortices that have been shed from the shear layer and convect downstream. Eventually, the vortex destabilizes and breaks into smaller structures, which results in mean flow reattachment. The shorter spacing of the vortices for 127 Hz case indicates that the vortices are shed more frequently than in the baseline case. Also, these vortices break down slightly earlier than baseline case. However, when forcing at 106 Hz, the vortex destabilization occurs substantially earlier, and the mean flow reattaches earlier than in the other cases.
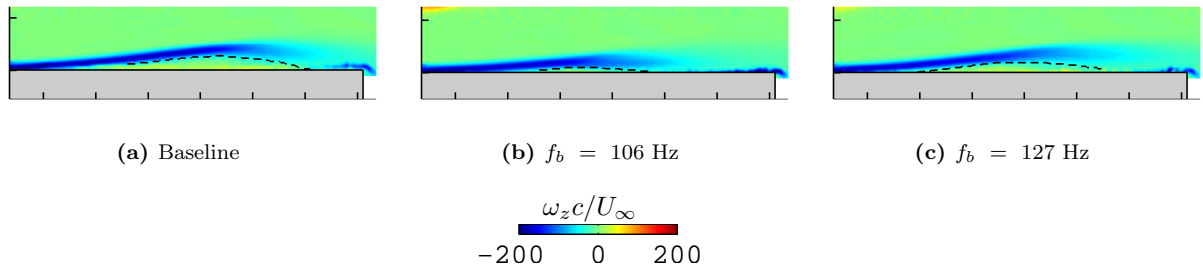
American Institute of Aeronautics and Astronautics

(a) Baseline **(b)** $f_b = 106$ Hz **(c)** $f_b = 127$ Hz

$$\omega_z c/U_\infty$$

$-200 \quad 0 \quad 200$

Figure 10: A comparison of the mean z-vorticity fields for the baseline separated flow, 106 Hz forcing frequency case, and 127 Hz forcing frequency case. The line of $\bar{u}/U_\infty = 0$ (dotted black line) is superimposed on the mean vorticity contours. The flat plate model is depicted in the plots for reference. The 106 Hz case exhibits the most reduced separation height of all of the forcing frequencies in this study.
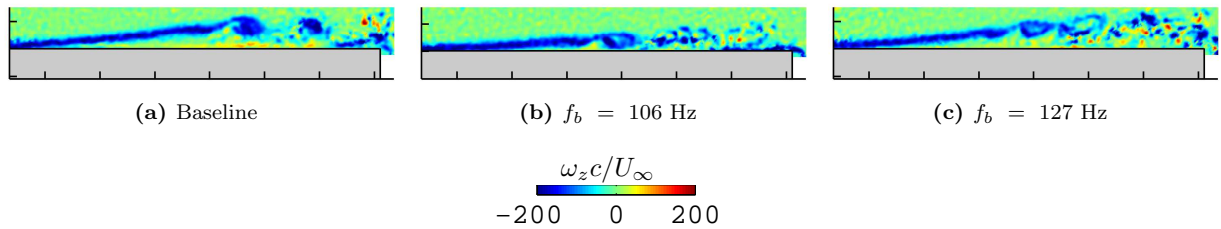

(a) Baseline **(b)** $f_b = 106$ Hz **(c)** $f_b = 127$ Hz

$$\omega_z c/U_\infty$$

$-200 \quad 0 \quad 200$

Figure 11: A comparison of select instantaneous z-vorticity fields for the baseline separated flow, 106 Hz forcing frequency case, and 127 Hz forcing frequency case. The flat plate model is depicted in the plots for reference. The 106 Hz case exhibits earlier vortex destabilization than the other cases. The 127 Hz case exhibits more frequent vortex shedding than the baseline case.

American Institute of Aeronautics and Astronautics

VI.   Conclusions

In this work, we explored the utility of DMD in informing open-loop control of flow separation in a series of canonical flow separation experiments. While it has been noted that DMD offers a "global" data analysis perspective for open-loop controller design that removes previously observed sensitivities to single probe analysis methods, these observations were reported in conjunction with numerical simulations where measurement noise is not a factor. Here, we applied the noise-aware TDMD technique [16] to snapshots of the velocity field gathered by TR-PIV, then compared the resulting analysis with the standard DMD algorithm. Dynamic characterizations of the experimental datsets from DMD and TDMD were compared to determine the sensitivity of the analysis in the context of open-loop controller design for separation control. For the datasets considered here, only small differences were observed between the dominant modes identified by DMD/TDMD. Since the dominant modes seem to be associated with the "best" open-loop forcing for suppressing the separation bubble, the advantages of TDMD over DMD in informing open-loop control design may be minimal; however, the noise-aware analysis indicates that measurement noise influences the less dominant modes to a greater extent, which can have implications in interpreting the dynamic characteristics of separated flows.

The advantages of the noise-aware framework are greatly pronounced in the context of low-storage streaming analysis techniques. In Section IV, we formulated STDMD—a noise-aware streaming variant of DMD—that can be used to study large and streaming datasets. The STDMD method introduced here greatly outperforms the original SDMD method (c.f., [18]) in extracting interpretable information from velocity field snapshots based on TR-PIV measurements from our canonical flow separation experiments. The performance of noise-robust streaming techniques will becomes especially important as the community pushes toward incorporating DMD-based techniques for model-predictive/adaptive control of flow separation.

Finally, we performed open-loop forcing experiments with a candidate set of forcing frequencies determined from the TDMD analysis. Forcing at the dominant DMD mode suppressed the separation bubble more than any of the other candidate frequencies. While a satisfying explanation of this observation requires further investigation, the observation is consistent with findings reported in previous numerical studies on open-loop forcing strategies informed by DMD analyses. Furthermore, since the noise-aware analysis techniques (i.e., TDMD and STDMD) give similar results, in this case, either analysis approach can be applied to snapshots of the velocity field to inform open-loop controller design; one only needs to identify the dominant dynamic mode. Future investigations will consider whether these claims are generalizable to other separation regimes as well (e.g., at different Re_c). If the observations reported here generalize to other flow regimes, then DMD-based techniques may be reliably used to inform open-loop separation control. Moreover, such a generalization, in conjunction with noise-aware STDMD technique introduced here, would provide further justification for using DMD-based techniques for model-predictive/adaptive control of separated flows.

VII.   Acknowledgments

References

[1] Seifert, A., Bachar, T., Koss, D., Shepshelovich, M., and Wygnanski, I., "Oscillatory Blowing: A Tool to Delay Boundary Layer Separation," *AIAA Journal*, Vol. 31, 1993, pp. 2052–2060.

[2] Seifert, A., Darabi, A., and Wygnanski, I., "Delay of Airfoil Stall by Periodic Excitation," *Journal of Aircraft*, Vol. 33, No. 4, 1996, pp. 691–698.

[3] Amitay, M., Smith, B. L., and Glezer, A., "Aerodynamic Flow Control Using Synthetic Jet Technology," *AIAA Paper 98-0208*, 1998.

[4] Chatlynne, E., Rumigny, N., Amitay, M., and Glezer, A., "Virtual Aero-Shaping of a Clark-Y Airfoil Using Synthetic Jet Actuators," *AIAA Paper 2001-0732*, 2001.

[5] Raju, R., Mittal, R., and Cattafesta, L., "Dynamics of Airfoil Separation Control Using Zero-Net Mass-Flux Forcing," *AIAA Journal*, Vol. 46, No. 12, 2008, pp. 3103–3115.

[6] Pern, N. J. and Jacob, J. D., "Comparison between Zero Mass Flux Flow Control Methods for Low Speed Airfoil Separation Control," *AIAA Paper 2005-4884*, 2005.

[7] Sosa, R., Artana, G., Moreau, E., and Touchard, G., "Stall Control at High Angle of Attack with Plasma Sheet Actuators," *Experiments in Fluids*, Vol. 42, 2007, pp. 143–167.

[8] Corke, T., Post, M., and Orlov, D., "Single Dielectric Barrier Discharge Plasma Enhanced Aerodynamics: Physics, Modeling, and Applications," *Experiments in Fluids*, Vol. 46, 2009, pp. 1–26.

[9] Little, J. and Samimy, M., "High-Lift Airfoil Separation with Dielectric Barrier Discharge Plasma Actuation," *AIAA Journal*, Vol. 48, No. 12, 2010, pp. 2884–2898.

[10] Little, J., Takashima, K., Nishihara, M., Adamovich, I., and Samimy, M., "Separation Control with Nanosecond-Pulse-Driven Dielectric Barrier Discharge Plasma Actuators," *AIAA Journal*, Vol. 50, No. 2, 2012, pp. 350–365.

[11] Mittal, R. and Kotapati, R. B., "Resonant Mode Interaction in a Canonical Separated Flow," *Proceedings of the IUTAM Symposium on Laminar-Turbulent Transition*, 2004.

[12] Mittal, R., Kotapati, R. B., and Cattafesta, L. N., "Numerical Study of Resonant Interactions and Flow Control in a Canonical Separated Flow," *AIAA Paper 2005-1261*, 2005.

[13] Kotapati, R. B., Mittal, R., Marxen, O., Ham, F., You, D., , and Cattafesta, L. N., "Nonlinear Dynamics and Synthetic-Jet-based Control of a Canonical Separated Flow," *Journal of Fluid Mechanics*, Vol. 654, 2010, pp. 65–97.

[14] Tu, J. H., Rowley, C. W., Aram, E., and Mittal, R., "Koopman Spectral Analysis of Separated Flow over a Finite-Thickness Flat Plate with Elliptical Leading Edge," *AIAA Paper 2011-38*, 2011.

[15] Griffin, J., Oyarzun, M., Cattafesta, L. N., Tu, J. H., Rowley, C. W., and Mittal, R., "Control of a Canonical Separated Flow," *AIAA Paper 2013-2968*, 2013.

[16] Hemati, M. S., Rowley, C. W., Deem, E. A., and Cattafesta, L. N., "De-Biasing the Dynamic Mode Decomposition for Applied Koopman Spectral Analysis of Noisy Datasets," *pre-print*, arXiv:1502.03854, 2015.

[17] Dawson, S. T. M., Hemati, M. S., Williams, M. O., and Rowley, C. W., "Characterizing and Correcting for the Effect of Sensor Noise in the Dynamic Mode Decomposition," *pre-print*, arXiv:1507.02264, 2015.

[18] Hemati, M. S., Williams, M. O., and Rowley, C. W., "Dynamic Mode Decomposition for Large and Streaming Datasets," *Physics of Fluids*, Vol. 26, No. 111701, 2014.

[19] Williams, M. O., Kevrekidis, I. G., and Rowley, C. W., "A Data-Driven Approximation of the Koopman Operator: Extending Dynamic Mode Decomposition," *Journal of Nonlinear Science*, Vol. 25, June 2015, pp. 1307–1346.

[20] Williams, M. O., Rowley, C. W., and Kevrekidis, I. G., "A Kernel-Based Approach to Data-Driven Koopman Spectral Analysis," *pre-print*, arXiv:1411.2260, 2014.

[21] DMDTools, http://z.umn.edu/dmdtools/, 2015.

[22] Holman, R., Utturkar, Y., Mittal, R., Smith, B. L., and Cattafesta, L., "Formation criterion for synthetic jets," *AIAA journal*, Vol. 43, No. 10, 2005, pp. 2110–2116.

[23] Melling, A., "Tracer Particles and Seeding for Particle Image Velocimetry," *Measurement Science and Technology*, Vol. 8, 1997, pp. 1406–1416.

[24] LaVision, "DaVis v8.1.x," 2013.

[25] Schmid, P. and Sesterhenn, J., "Dynamic Mode Decomposition of Numerical and Experimental Data," *61st Annual Meeting of the APS Division of Fluid Dynamics*, 2008.

[26] Schmid, P., "Dynamic Mode Decomposition of Numerical and Experimental Data," *Journal of Fluid Mechanics*, Vol. 656, 2010, pp. 5–28.

[27] Tu, J. H., Rowley, C. W., Luchtenburg, D. M., Brunton, S. L., and Kutz, J. N., "On Dynamic Mode Decomposition: Theory and Applications," *Journal of Computational Dynamics*, Vol. 1, No. 2, December 2014, pp. 391–421.

[28] Duke, D., Honnery, D., and Soria, J., "Experimental Investigation of Nonlinear Instabilities in Annular Liquid Sheets," *Journal of Fluid Mechanics*, Vol. 691, 2012, pp. 594–604.

[29] Duke, D., Soria, J., and Honnery, D., "An Error Analysis of the Dynamic Mode Decomposition," *Experiments in Fluids*, Vol. 52, No. 2, 2012, pp. 529–542.

[30] Schmid, P., "Application of the Dynamic Mode Decomposition to Experimental Data," *Experiments in Fluids*, Vol. 50, 2011, pp. 1123–1130.

[31] Schmid, P., Li, L., Juniper, M., and Pust, O., "Applications of the Dynamic Mode Decomposition," *Theoretical and Computational Fluid Dynamics*, Vol. 25, 2011, pp. 249–259.

[32] Semeraro, O., Bellani, G., and Lundell, F., "Analysis of Time-Resolved PIV Masurements of a Confined Turbulent Jet using POD and Koopman Modes," *Experiments in Fluids*, Vol. 53, 2012, pp. 1203–1220.

[33] Wynn, A., Pearson, D., Ganapathisubramani, B., and Goulart, P., "Optimal Mode Decomposition for Unsteady Flows," *Journal of Fluid Mechanics*, Vol. 733, 2013, pp. 473–503.

[34] Jovanović, M. R., Schmid, P. J., and Nichols, J. W., "Sparsity Promoting Dynamic Mode Decomposition," *Physics of Fluids*, Vol. 26, No. 024103, 2014.

[35] Proctor, J. L., Brunton, S. L., and Kutz, J. N., "Dynamic Mode Decomposition with Control," *pre-print*, arXiv:1409.6358, 2014.